Power Engineering and Engineering Thermophysics
https://www.acadlore.com/journals/PEET

FLT-HPM for Two-dimensional Transient Natural Convection in a Horizontal Cylindrical Concentric Annulus

Yasir Ahmed Abdulameer*, Abdulsattar Jaber Ali Al-Saif

Department of Mathematics, College of Education for Pure Science, Basrah University, 61001 Basrah, Iraq

* Correspondence: Yasir Ahmed Abdulameer (pepg.yasir.ahmed@uobasrah.edu.iq)

Received: 03-18-2023 **Revised:** 04-25-2023 **Accepted:** 05-18-2023

Citation: Y. A. Abdulameer and A. J. A. Al-Saif, "FLT-HPM for two-dimensional transient natural convection in a horizontal cylindrical concentric annulus," *Power Eng. Eng. Thermophys.*, vol. 2, no. 3, pp. 120–138, 2023. https://doi.org/10.56578/peet020301.

Abstract: A hybrid procedure FLT-HPM was proposed in this study, by combining the homotopy perturbation method (HPM) with Fourier transform and Laplace transform which aimed to find an approximate analytical solution to the problem of two-dimensional transient natural convection in a horizontal cylindrical concentric annulus bounded by two isothermal surfaces. The effect of the Grashof number, Prandtl number, and the radius ratio on fluid flow (air) and heat transfer with different values awreas discussed. Moreover, the velocity distributions and the mean Nusselt numbers were studied, and the Nusselt numbers were used to represent local and general heat transfer rates. Finally, the convergence of FLT-HPM was tested theoretically through the proof of some theorems. In addition, these theorems were applied to the results of the new solutions obtained using FLT-HPM.

Keywords: FLT-HPM; Homotopy perturbation method; Fourier transform; Laplace transform; Natural convection; Cylindrical annulus

1 Introduction

Researchers and scientists have been interested in the heat transfer theory of natural convection recently because of its wide applications in various science and technology fields, including aircraft cabin insulation, nuclear reactors, solar collector sensors, heat storage systems, power transmission cables, cooling of electronic components, etc [1–5]. Two-dimensional transient natural convection between two concentric circular horizontal cylinders is one of the most famous problems of natural convection, and has attracted the attention of quite a few researchers. Among the first researchers to provide experimental solutions to this problem, Crawford and Lemlich [6] carried out a numerical study and succeeded in approximating the steady-state differential equations with appropriate difference equations. Moreover, the effect of diameter ratios at 2, 8 and 57 was discussed with 0.7 as the Prandtl number. This study paved the way for many authors and researchers who succeeded in finding numerical and analytical solutions to the above problem. For example, Mack and Bishop [7] used the Rayleigh number power series to solve the problem of natural convection between two concentric horizontal cylinders with slight temperature difference. In their analytical study, the effect of Prandtl number, Rayleigh number and radius ratio on streamline formation, local heat transfer rates, velocity and temperature distributions were discussed. Kuehn and Goldstein [2] introduced experimental and theoretical-numerical studies. In the experimental study, the Mach-Zehnder interferometer was used to locate temperature distributions and coefficients of local heat-transfer. In addition, the governing invariant property equations were solved numerically using the finite difference method. The comparisons between experimental and numerical results under similar conditions illustrated good consistence. Tsui and Tremblay [4] conducted a theoretical-numerical study, and discussed the effect of both the Grashof number from 7×10^2 to 9×10^4 and diameter ratio variations of 1.2, 1.5 and 2 with 0.7 as the Prandtl number. Pop et al. [8] obtained an approximate analytical solution to the presented problem. The method of matched asymptotic expansions was used, which obtained the solutions for three regions (core, inner and outer boundary layers) in a short time. It was found that the solution was distinct from the steady state solution. Hassan and Al-lateef [9] conducted a numerical study in which the energy and vorticity equation was solved using the alternating direction implicit (ADI) method, and the stream function equation was solved using the successive over relaxation (SOR) method. The results of the numerical solutions were discussed, based on the difference in diameter ratios of 1.2, 1.5 and 2, the effect of the Grashof number ranging from

10^2 to 10^5 and different values of the Prandtl number. Touzani et al. [10] presented a numerical study of natural convection in a horizontal annulus with two heating blocks, which found that heat transfer increased significantly at the upper region of the annulus. In addition, it was noted that the block helped improve the heat transfer in general. Al-Saif and Al-Griffi [11] proposed a new procedure by combining the HPM with Yang transform (YT), which succeeded in finding analytical approximate solutions to the problem of two-dimensional transient natural convection in a concentric cylindrical horizontal annulus bounded by two isothermal surfaces. The effect of different values of the Grashof numbers and the radius ratio on heat transfer and fluid flow (air) with 0.7 as the Prandtl number was studied.

Many iterative methods have been used to find analytical solutions to non-linear flow problems, especially natural convection. However, due to high computational operations requiring lots of time and effort, almost most of these methods have some difficulties to obtain the desired solution, such as HPM [12], Homotopy Analysis Method (HAM) [13] and Differential Quadrature Method (DQM) [14, 15]. In addition, various integral transformations, such as Yang transform, Laplace transform, and Fourier transform, can be used to find analytical solutions to linear problems. But it is often difficult to use these methods to obtain analytical solutions to some non-linear problems. Therefore, this study aimed to create a new procedure to avoid the above difficulties. In recent years, researchers have noted that combined integrative transform methods with iterative methods may help address the difficulties arising from use of an individual method. Moreover, this study proposed to combine the Fourier and Laplace transforms with the HPM to get a new algorithm FLT-HPM. Apart from the above literature review, no one has used this FLT-HPM to solve the problems of natural convection, in particular the current problem. This study presented FLT-HPM in order to find approximate analytical solutions to the two-dimensional transient natural convection problem in a concentric horizontal cylindrical annulus. Moreover, the problem was divided into three regions, the inner boundary layer (located near the inner cylinder), the outer boundary layer (located near the outer cylinder), and core region (located between the two layers). The analytical solutions of those regions were found using the FLT-HPM. In addition, the convergence analysis of FLT-HPM was studied analytically and experimentally by formulating and proving some theorems. These theorems were applied to the results of the obtained analytical solutions. Related tables and graphs showed the necessity, importance and benefit of using FLT-HPM. Finally, the results showed the accuracy and efficiency of FLT-HPM, which were in consistent with the results of previously published studies [1, 4, 9].

2 HPM

In 1998, researcher He [16, 17] introduced HPM, which was characterized by its ability to solve many linear and non-linear differential and integral equations. HPM is highly accurate and efficient and has proven effective in solving many non-linear problems with wide applications in various fields of life. When using HPM, the solution was assumed as the sum of an infinite convergent series [18]. The general form of the following non-linear differential equation was used to display the basic idea of FLT-HPM:

$$A(u) - g(r) = 0, r \in \Omega \tag{1}$$

And it was associated with the following boundary conditions:

$$B\left(u, \frac{\partial u}{\partial n}\right) = 0, r \in \Gamma \tag{2}$$

where, u is the unknown function, $g(r)$ is a known analytic function, A is the general differential operator, B is the boundary operator, and Γ is the boundary of the domain Ω. The operator A was divided into linear operator L and non-linear operator N. Moreover, Eq. (1) was rewritten as:

$$L(u) + N(u) - q(r) = 0 \tag{3}$$

Based on the basic idea of HPM, the homotopy $U(r, p) : \Omega \times [0, 1] \to R$ was defined by the following formula:

$$H(U, p) = (1 - p)\left[L(U) - L\left(u_0\right)\right] + p[A(U) - g(r)] = 0 \tag{4}$$

or

$$H(U, p) = L(U) - L\left(u_0\right) + pL\left(u_0\right) + p[N(U) - g(r)] = 0 \tag{5}$$

where, $p \in [0,1]$ is the impeding parameter and u_0 is an initial solution of Eq. (1), satisfying the boundary conditions of Eq. (2). It was clear that Eq. (4) or (5) satisfied the conditions of homotopy as follows:

$$\left.\begin{array}{c} H(U,0) = L(U) - L\left(u_0\right) = 0, \\ H(U,1) = A(U) - g(r) = 0. \end{array}\right\} \tag{6}$$

The solution of Eq. (4) or (5) was assumed as a power series for p as follows:

$$U = \sum_{j=0}^{\infty} p^j U_j \tag{7}$$

By setting $p = 1$, the approximate solution of Eq. (1) was given as follows:

$$u = \lim_{p \to 1} U = \sum_{j=0}^{\infty} U_j \tag{8}$$

3 Basic Algorithm of FLT-HPM

This section aimed to develop the HPM to obtain a more advanced hybrid procedure FLT-HPM, using the Fourier transform and Laplace transform. The non-linear differential equation was written in the following form to fully explain FLT-HPM:

$$\frac{\partial^n}{\partial r_1^n}\left(\frac{\partial^m}{\partial r_2^m} U\right) + R(U) + N(U) = g\left(r_1, r_2\right), r_1, r_2 \in \Omega \tag{9}$$

where, R and N are the linear and non-linear differential operators respectively, and $g\left(r_1, r_2\right)$ is the source term. Accordingly, basic steps of this algorithm were as follows:

After applying the Fourier transform to r_1 for both sides of Eq. (9), there were:

$$\mathcal{F}\left[\frac{\partial^n}{\partial r_1^n}\left(\frac{\partial^m}{\partial r_2^m} U\right)\right] + \mathcal{F}\left[R(U) + N(U) - g\left(r_1, r_2\right)\right] = 0, r_1, r_2 \in \Omega \tag{10}$$

where, $\mathcal{F}[g(t)] = \mathcal{F}(\omega) = \int_{-\infty}^{\infty} g(t) e^{-i\omega t} dt$.

The differentiation property of the Fourier transform was used, which obtained:

$$(i\omega)^n \mathcal{F}\left[\frac{\partial^m}{\partial r_2^m} U\right] + \mathcal{F}\left[R(U) + N(U) - g\left(r_1, r_2\right)\right] = 0 \tag{11}$$

Eq. (11) was rearranged as:

$$\mathcal{F}\left[\frac{\partial^m}{\partial r_2^m} U\right] + \frac{1}{(i\omega)^n} \mathcal{F}\left[R(U) + N(U) - g\left(r_1, r_2\right)\right] = 0 \tag{12}$$

The inverse Fourier transform for both sides of Eq. (12) was taken, which obtained:

$$\frac{\partial^m}{\partial r_2^m} U + \mathcal{F}^{-1}\left[\frac{1}{(i\omega)^n} \mathcal{F}\left[R(U) + N(U) - g\left(r_1, r_2\right)\right]\right] = 0 \tag{13}$$

HPM was used, which obtained:

$$(1-p)\left[\frac{\partial^m}{\partial r_2^m} U - \frac{\partial^m}{\partial r_2^m} u_0\right] + p\left[\frac{\partial^m}{\partial r_2^m} U + \mathcal{F}^{-1}\left\{\frac{1}{(i\omega)^n} \mathcal{F}\left[R(U) + N(U) - g\left(r_1, r_2\right)\right]\right\}\right] = 0 \tag{14}$$

After Eq. (14) was rearranged, the following was deduced:

$$\frac{\partial^m}{\partial r_2^m}U = \frac{\partial^m}{\partial r_2^m}u_0 - p\frac{\partial^m}{\partial r_2^m}u_0 - p\left[\mathcal{F}^{-1}\left\{\frac{1}{(i\omega)^n}\mathcal{F}\left[R(U)+N(U)-g\left(r_1,r_2\right)\right]\right\}\right] \tag{15}$$

The Laplace transform was applied to r_2 on both sides of Eq. (15), which obtained:

$$\mathcal{L}\left[\frac{\partial^m}{\partial r_2^m}U\right] = \mathcal{L}\left[\frac{\partial^m}{\partial r_2^m}u_0\right] - p\mathcal{L}\left[\frac{\partial^m}{\partial r_2^m}u_0 + \mathcal{F}^{-1}\left\{\frac{1}{(i\omega)^n}\mathcal{F}\left[R(U)+N(U)-g\left(r_1,r_2\right)\right]\right\}\right] \tag{16}$$

where, $\mathcal{L}[g(t)] = \mathcal{L}(s) = \int_0^\infty g(t)e^{-st}dt$.

The differentiation property of the Laplace transform was used, which obtained:

$$\mathcal{L}[U] = \frac{1}{s^m}\sum_{k=0}^{m-1}s^{m-k-1}U^{(k)}(0) + \frac{1}{s^n}\mathcal{L}\left[\frac{\partial^m u_0}{\partial r_2^m}\right] - \frac{p}{s^n}\mathcal{L}\left[\frac{\partial^m u_0}{\partial r_2^m} + \mathcal{F}^{-1}\left\{\frac{1}{(i\omega)^n}\mathcal{F}\left[\begin{array}{c} R(U)+N(U) \\ -g\left(r_1,r_2\right)\end{array}\right]\right\}\right] \tag{17}$$

The inverse Laplace transform for both sides of Eq. (17) was taken, which obtained:

$$U = \mathcal{L}^{-1}\left[\frac{1}{s^m}\sum_{k=0}^{m-1}s^{m-k-1}U^{(k)}(0)\right] + \mathcal{L}^{-1}\left[\begin{array}{c} \frac{1}{s^m}\mathcal{L}\left[\frac{\partial^m}{\partial r_2^m}u_0\right] - \frac{p}{s^m}\mathcal{L}\left[\frac{\partial^m}{\partial r_2^m}u_0\right] - \\ \frac{p}{s^m}\mathcal{L}\left\{\mathcal{F}^{-1}\left[\frac{1}{(i\omega)^n}\mathcal{F}\left[\begin{array}{c} R(U)+N(U) \\ -g\left(r_1,r_2\right)\end{array}\right]\right]\right\}\end{array}\right] \tag{18}$$

Based on the assumption of HPM, the following was obtained:

$$U = \sum_{j=0}^{\infty}p^j U_j \tag{19}$$

And the nonlinear terms were decomposed as:

$$N(U) = \sum_{j=0}^{\infty}p^j H_j \tag{20}$$

where, $H_j(U)$ is the He's polynomials [19] given by:

$$H_j\left(U_0,U_1,U_2,\ldots,U_j\right) = \frac{1}{j!}\frac{\partial^j}{\partial p^j}\left[N\left(\sum_{i=0}^{\infty}p^i U_i\right)\right]_{p=0}, j = 0,1,2,3,\ldots \tag{21}$$

Eqs. (19) and (20) were substituted into Eq. (18), which obtained:

$$\sum_{j=0}^{\infty}p^j U_j = \mathcal{L}^{-1}\left[\frac{\sum_{k=0}^{m-1}s^{m-k-1}U^{(k)}(0)}{s^m}\right] + \mathcal{L}^{-1}\left[\begin{array}{c} \frac{1}{s^m}\mathcal{L}\left[\frac{\partial^m}{\partial r_2^m}u_0\right] - \frac{p}{s^m}\mathcal{L}\left[\frac{\partial^m}{\partial r_2^m}u_0\right] - \\ \frac{p}{s^m}\mathcal{L}\left\{\mathcal{F}^{-1}\left[\frac{1}{(i\omega)^n}\mathcal{F}\left[\begin{array}{c} R\left(\sum_{j=0}^{\infty}p^j U_j\right)+ \\ \sum_{j=0}^{\infty}p^j H_j - g\left(r_1,r_2\right)\end{array}\right]\right]\right\}\end{array}\right] \tag{22}$$

Coefficients of the same powers of p were compared, which obtained:

$$p^0 : U_0 = \mathcal{L}^{-1}\left[\frac{1}{s^m}\sum_{k=0}^{m-1}s^{m-k-1}U^{(k)}(0)\right] + \mathcal{L}^{-1}\left[\frac{1}{s^m}\mathcal{L}\left[\frac{\partial^m}{\partial r_2^m}u_0\right]\right] \tag{23}$$

$$p^1 : U_1 = \mathcal{L}^{-1}\left[-\frac{1}{s^m}\mathcal{L}\left[\frac{\partial^m}{\partial r_2^m}u_0\right] - \frac{1}{s^n}\mathcal{L}\left\{\mathcal{F}^{-1}\left[\frac{1}{(i\omega)^n}\mathcal{F}\left[R\left(U_0\right)+H_0-g\left(r_1,r_2\right)\right]\right]\right\}\right] \tag{24}$$

$$p^2 : U_2 = \mathcal{L}^{-1}\left[-\frac{1}{s^m}\mathcal{L}\left\{\mathcal{F}^{-1}\left[\frac{1}{(i\omega)^n}\mathcal{F}\left[R\left(U_1\right)+H_1\right]\right]\right\}\right] \tag{25}$$

$$p^j : U_j = \mathcal{L}^{-1}\left[-\frac{1}{s^m}\mathcal{L}\left\{\mathcal{F}^{-1}\left[\frac{1}{(i\omega)^n}\mathcal{F}\left[R\left(U_{j-1}\right)+H_{j-1}\right]\right]\right\}\right] \tag{26}$$

Taking $p = 1$, then the analytical approximate solution u was given by:

$$u = \lim_{p\to 1} U = \sum_{j=0}^{\infty} U_j \tag{27}$$

4 Mathematical Formulation of Governing Equation

The Newtonian fluid was taken into consideration in two concentric horizontal circular cylinders enclosed by two isothermal surfaces. Figure 1 shows the following: (a) both fluid motion and temperature distribution are two-dimensional; (b) fluid is incompressible and viscous; (c) the friction heating is almost too slight, and (d) the properties of fluid are constant except that its density changes with temperature.

Therefore, the governing mathematical equations were presented using the Boussinesq approximation as follows [4]:

$$\frac{\partial \widehat{U}}{\partial \hat{x}} + \frac{\partial \hat{V}}{\partial \hat{y}} = 0 \tag{28}$$

$$\frac{\partial \widehat{U}}{\partial \hat{t}} + \widehat{U}\frac{\partial \widehat{U}}{\partial \hat{x}} + \hat{V}\frac{\partial \widehat{U}}{\partial \hat{y}} = \left(\frac{-1}{\rho}\right)\frac{\partial \hat{P}}{\partial \hat{x}} + \hat{v}\left(\frac{\partial^2 \hat{U}}{\partial \hat{x}^2} + \frac{\partial^2 \hat{U}}{\partial \hat{y}^2}\right) \tag{29}$$

$$\frac{\partial \hat{V}}{\partial \hat{t}} + \widehat{U}\frac{\partial \hat{V}}{\partial \hat{x}} + \hat{V}\frac{\partial \hat{V}}{\partial \hat{y}} = \left(\frac{-1}{\rho}\right)\frac{\partial \hat{P}}{\partial \hat{y}} + \hat{v}\left(\frac{\partial^2 \hat{V}}{\partial \hat{x}^2} + \frac{\partial^2 \hat{V}}{\partial \hat{y}^2}\right) + \hat{g}\hat{\alpha}\left(\hat{T} - \hat{T}_o\right) \tag{30}$$

$$\frac{\partial \hat{T}}{\partial \hat{t}} + \hat{U}\frac{\partial \hat{T}}{\partial \hat{x}} + \hat{V}\frac{\partial \hat{T}}{\partial \hat{y}} = \hat{k}\left(\frac{\partial^2 \hat{T}}{\partial \hat{x}^2} + \frac{\partial^2 \hat{T}}{\partial \hat{y}^2}\right) \tag{31}$$

where, $\hat{U}$ and $\hat{V}$ are the components of velocity in $\hat{x}$ and $\hat{y}$ directions; $\hat{T}$ is the temperature, $\hat{g}$ is the gravity acceleration, $\hat{v}$ is the kinematic viscosity, ρ is the density, $\hat{\alpha}$ is the thermal expansion coefficient, and $\hat{k}$ is the thermal diffusivity.

To facilitate the solution of the problem, $\hat{y}$ in Eq. (29) and $\hat{x}$ in Eq. (30) were differentiated, with one of the two equations subtracted, and the definition of vorticity function $\left(\hat{\mathcal{G}} = \frac{\partial \widehat{V}}{\partial \hat{x}} + \frac{\partial \widehat{U}}{\partial \hat{y}}\right)$ was used with the pressure omitted, which reduced the two equations to the vorticity-stream form. In addition, the Cartesian coordinate system was converted to the polar one. Then the dimensionless set was used to convert the problem from dimensional to non-dimensional form as follows:

$$U = \frac{\widehat{U}\widehat{L}}{\hat{v}}, V = \frac{\widehat{V}\widehat{L}}{\hat{v}}, \psi = \frac{\widehat{\psi}}{\hat{v}}, r = \frac{\hat{r}}{\widehat{L}}, t = \frac{\hat{t}\hat{v}}{\widehat{L}^2}, \mathcal{G} = \frac{\widehat{L}^2\hat{\mathcal{G}}}{\hat{v}}, T = \frac{\widehat{T} - \widehat{T}_o}{\widehat{T}_h - \widehat{T}_c}, \nabla^2 = \widehat{L}^2\widehat{\nabla}^2 \tag{32}$$

The non-dimensional governing equations were given by the following stream-vorticity formulas:

$$\frac{\partial \mathcal{G}}{\partial t} + U\frac{\partial \mathcal{G}}{\partial r} + \frac{1}{r}V\frac{\partial \mathcal{G}}{\partial \theta} = Gr\left(\cos(\theta)\frac{\partial T}{\partial r} - \frac{\sin(\theta)}{r}\frac{\partial T}{\partial \theta}\right) + \nabla^2\mathcal{G} \tag{33}$$

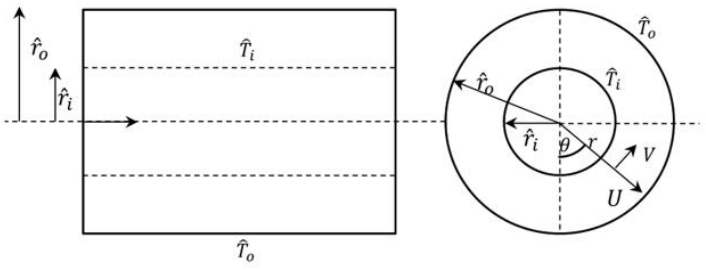

Figure 1. Physical flow geometry and coordinate system

$$\frac{\partial T}{\partial t} + U\frac{\partial T}{\partial r} + \frac{1}{r}V\frac{\partial T}{\partial \theta} = \frac{1}{Pr}\nabla^2 T \tag{34}$$

$$\mathcal{G} = -\nabla^2\psi \tag{35}$$

$$V = -\frac{\partial \psi}{\partial r}, U = \frac{1}{r}\frac{\partial \psi}{\partial \theta} \tag{36}$$

The above system was subject to the following initial and boundary conditions:

$$\mathcal{G} = \psi = T = 0 \tag{37}$$

$$\left.\begin{array}{ll} \psi & = \frac{\partial \psi}{\partial r} = \frac{1}{r}\frac{\partial \psi}{\partial \theta} = 0, \text{ at } r = R_i, r = R_o, \\ T & = 1 \text{ at } r = R_i, \\ T & = 0 \text{ at } r = R_0. \end{array}\right\} \tag{38}$$

where, $\hat{L}$ is the gap of annulus, R_i and R_o are the ratios of inner and outer radius to the gap, respectively, Pr is the Prandtl number, Gr is the Grashof number, U is the radial velocity, V is the tangent velocity, T is the temperature, ψ is the stream function, $\mathcal{G}$ is the vorticity function, subscripts i, o, c and h are inner, outer, cold and hot, respectively.

5 Application of FLT-HPM

To apply FLT-HPM, Eqs. (35) and (36) were first substituted into Eqs. (33) and (34) to get the following system:

$$\frac{\partial}{\partial t}\left(\nabla^2\psi\right) + Gr\left(\cos(\theta)\frac{\partial T}{\partial r} - \frac{\sin(\theta)}{r}\frac{\partial T}{\partial \theta}\right) - \nabla^4\psi - \frac{1}{r}\left(\frac{\partial \psi}{\partial r}\frac{\partial}{\partial \theta}\left(\nabla^2\psi\right) - \frac{\partial \psi}{\partial \theta}\frac{\partial}{\partial r}\left(\nabla^2\psi\right)\right) = 0 \tag{39}$$

$$\frac{\partial T}{\partial T} - \frac{1}{Pr}\nabla^2 T - \frac{1}{r}\left(\frac{\partial \psi}{\partial r}\frac{\partial T}{\partial \theta} - \frac{\partial \psi}{\partial \theta}\frac{\partial T}{\partial r}\right) = 0 \tag{40}$$

$\nabla^2 = \frac{\partial^2}{\partial r^2} + \frac{1}{r}\frac{\partial}{\partial r} + \frac{1}{r^2}\frac{\partial^2}{\partial \theta^2}$ was substituted into Eq. (39), which obtained:

$$\frac{\partial}{\partial t}\left(\frac{\partial^2\psi}{\partial r^2} + \frac{1}{r}\frac{\partial \psi}{\partial r} + \frac{1}{r^2}\frac{\partial^2\psi}{\partial \theta^2}\right) + \mathrm{Gr}\left(\cos(\theta)\frac{\partial T}{\partial r} - \frac{\sin(\theta)}{r}\frac{\partial T}{\partial \theta}\right) - \nabla^4\psi - \frac{1}{r}\left(\frac{\partial \psi}{\partial r}\frac{\partial\left(\nabla^2\psi\right)}{\partial \theta} - \frac{\partial \psi}{\partial \theta}\frac{\partial\left(\nabla^2\psi\right)}{\partial r}\right) = 0 \tag{41}$$

Eq. (41) was rewritten as:

$$\frac{\partial^2\psi}{\partial r \partial t} + \frac{\partial}{\partial t}\left(\frac{\partial^2\psi}{\partial r^2}r + \frac{1}{r}\frac{\partial^2\psi}{\partial \theta^2}\right) + Gr\left(r\cos(\theta)\frac{\partial T}{\partial r} - \sin(\theta)\frac{\partial T}{\partial \theta}\right) - r\nabla^4\psi - \left(\frac{\partial \psi}{\partial r}\frac{\partial\left(\nabla^2\psi\right)}{\partial \theta} - \frac{\partial \psi}{\partial \theta}\frac{\partial\left(\nabla^2\psi\right)}{\partial r}\right) = 0 \tag{42}$$

Then the basic steps of FLT-HPM were as follows:
The Fourier transform was applied to r for both sides of Eq. (42), which obtained:

$$\mathcal{F}\left[\frac{\partial^2\psi}{\partial r\partial t}\right]+\mathcal{F}\left[\begin{array}{c}\frac{\partial}{\partial t}\left(\frac{\partial^2\psi}{\partial r^2}r+\frac{1}{r}\frac{\partial^2\psi}{\partial\theta^2}\right)+Gr\left(r\cos(\theta)\frac{\partial T}{\partial r}-\sin(\theta)\frac{\partial T}{\partial\theta}\right)\\-\left(\nabla^4\psi\right)r-\left(\frac{\partial\psi}{\partial r}\frac{\partial}{\partial\theta}\left(\nabla^2\psi\right)-\frac{\partial\psi}{\partial\theta}\frac{\partial}{\partial r}\left(\nabla^2\psi\right)\right)\end{array}\right]=0 \tag{43}$$

The differentiation property of the Fourier transform was used, which obtained:

$$\mathcal{F}\left[\frac{\partial\psi}{\partial t}\right]+\frac{1}{i\omega}\mathcal{F}\left[\begin{array}{c}\frac{\partial}{\partial t}\left(\frac{\partial^2\psi}{\partial r^2}r+\frac{1}{r}\frac{\partial^2\psi}{\partial\theta^2}\right)+Gr\left(r\cos(\theta)\frac{\partial T}{\partial r}-\sin(\theta)\frac{\partial T}{\partial\theta}\right)\\-\left(\nabla^4\psi\right)r-\left(\frac{\partial\psi}{\partial r}\frac{\partial}{\partial\theta}\left(\nabla^2\psi\right)-\frac{\partial\psi}{\partial\theta}\frac{\partial}{\partial r}\left(\nabla^2\psi\right)\right)\end{array}\right]=0 \tag{44}$$

The inverse Fourier transform for both sides of Eq. (44) was taken, which obtained:

$$\frac{\partial\psi}{\partial t}+\mathcal{F}^{-1}\left[\frac{1}{i\omega}\mathcal{F}\left\{\begin{array}{c}\frac{\partial}{\partial t}\left(\frac{\partial^2\psi}{\partial r^2}r+\frac{1}{r}\frac{\partial^2\psi}{\partial\theta^2}\right)+Gr\left(r\cos(\theta)\frac{\partial T}{\partial r}-\sin(\theta)\frac{\partial T}{\partial\theta}\right)\\-\left(\nabla^4\psi\right)r-\left(\frac{\partial\psi}{\partial r}\frac{\partial}{\partial\theta}\left(\nabla^2\psi\right)-\frac{\partial\psi}{\partial\theta}\frac{\partial}{\partial r}\left(\nabla^2\psi\right)\right)\end{array}\right\}\right]=0 \tag{45}$$

The HPM was used for Eqs. (40) and (45), which obtained:

$$(1-p)\left[\frac{\partial\psi}{\partial t}-\psi_0^*\right]+p\left[\mathcal{F}^{-1}\left[\frac{1}{i\omega}\mathcal{F}\left\{\begin{array}{c}\frac{\partial\psi}{\partial t}+\\\frac{\partial}{\partial t}\left(\frac{\partial^2\psi}{\partial r^2}r+\frac{1}{r}\frac{\partial^2\psi}{\partial\theta^2}\right)+\mathrm{Gr}\left(r\cos(\theta)\frac{\partial T}{\partial r}-\sin(\theta)\frac{\partial T}{\partial\theta}\right)\\-\left(\nabla^4\psi\right)r-\left(\frac{\partial\psi}{\partial r}\frac{\partial}{\partial\theta}\left(\nabla^2\psi\right)-\frac{\partial\psi}{\partial\theta}\frac{\partial}{\partial r}\left(\nabla^2\psi\right)\right)\end{array}\right\}\right]\right]=0 \tag{46}$$

$$(1-p)\left[\frac{\partial T}{\partial t}-T_0^*\right]+p\left[\frac{\partial T}{\partial t}-\frac{1}{Pr}\nabla^2T-\frac{1}{r}\left(\frac{\partial\psi}{\partial r}\frac{\partial T}{\partial\theta}-\frac{\partial\psi}{\partial\theta}\frac{\partial T}{\partial r}\right)\right]=0 \tag{47}$$

The above system was rearranged as:

$$\frac{\partial\psi}{\partial t}-\psi_0^*+p\psi_0^*+p\mathcal{F}^{-1}\left[\frac{1}{i\omega}\mathcal{F}\left\{\begin{array}{c}\frac{\partial}{\partial t}\left(\frac{\partial^2\psi}{\partial r^2}r+\frac{1}{r}\frac{\partial^2\psi}{\partial\theta^2}\right)+Gr\left(r\cos(\theta)\frac{\partial T}{\partial r}-\sin(\theta)\frac{\partial T}{\partial\theta}\right)\\-\left(\nabla^4\psi\right)r-\left(\frac{\partial\psi}{\partial r}\frac{\partial}{\partial\theta}\left(\nabla^2\psi\right)-\frac{\partial\psi}{\partial\theta}\frac{\partial}{\partial r}\left(\nabla^2\psi\right)\right)\end{array}\right\}\right]=0 \tag{48}$$

$$\frac{\partial T}{\partial t}-T_0^*+pT_0^*-p\left[\frac{1}{Pr}\nabla^2T+\frac{1}{r}\left(\frac{\partial\psi}{\partial r}\frac{\partial T}{\partial\theta}-\frac{\partial\psi}{\partial\theta}\frac{\partial T}{\partial r}\right)\right]=0 \tag{49}$$

The Laplace transform was applied to t on both sides of Eqs. (48) and (49), which obtained:

$$\mathcal{L}[\psi]=\frac{1}{s}\psi(0)+\frac{1}{s}\mathcal{L}\left[\psi_0^*\right]-\frac{1}{s}\mathcal{L}\left[p\psi_0^*+p\mathcal{F}^{-1}\left\{\frac{1}{i\omega}\mathcal{F}\left[\begin{array}{c}\frac{\partial}{\partial t}\left(\frac{\partial^2\psi}{\partial r^2}\right)r+\frac{1}{r}\frac{\partial}{\partial t}\left(\frac{\partial^2\psi}{\partial\theta^2}\right)-\left(\nabla^4\psi\right)r\\+Gr\left(r\cos(\theta)\frac{\partial T}{\partial r}-\sin(\theta)\frac{\partial T}{\partial\theta}\right)\\-\left(\frac{\partial\psi}{\partial r}\frac{\partial}{\partial\theta}\left(\nabla^2\psi\right)-\frac{\partial\psi}{\partial\theta}\frac{\partial}{\partial r}\left(\nabla^2\psi\right)\right)\end{array}\right]\right\}\right] \tag{50}$$

$$\mathcal{L}[T]=\frac{1}{S}T(0)+\frac{1}{S}\mathcal{L}\left[T_0^*\right]-\frac{1}{S}\mathcal{L}\left[pT_0^*-p\left\{\frac{1}{Pr}\nabla^2T+\frac{1}{r}\left(\frac{\partial\psi}{\partial r}\frac{\partial T}{\partial\theta}-\frac{\partial\psi}{\partial\theta}\frac{\partial T}{\partial r}\right)\right\}\right] \tag{51}$$

After taking the inverse Laplace transform for both sides of Eqs. (50) and (51), the following was deduced:

$$\psi=\mathcal{L}^{-1}\left[\frac{1}{s}\psi(0)+\frac{1}{s}\mathcal{L}\left[\psi_0^*\right]-\frac{p}{s}\mathcal{L}\left(\psi_0^*+\mathcal{F}^{-1}\left[\frac{1}{i\omega}\mathcal{F}\left\{\begin{array}{c}\frac{\partial}{\partial t}\left(\frac{\partial^2\psi}{\partial r^2}\right)r+\frac{1}{r}\frac{\partial}{\partial t}\left(\frac{\partial^2\psi}{\partial\theta^2}\right)-\left(\nabla^4\psi\right)r\\+Gr\left(r\cos(\theta)\frac{\partial T}{\partial r}-\sin(\theta)\frac{\partial T}{\partial\theta}\right)\\-\left(\frac{\partial\psi}{\partial r}\frac{\partial}{\partial\theta}\left(\nabla^2\psi\right)-\frac{\partial\psi}{\partial\theta}\frac{\partial}{\partial r}\left(\nabla^2\psi\right)\right)\end{array}\right\}\right]\right)\right] \tag{52}$$

$$T=\mathcal{L}^{-1}\left[\frac{1}{s}T(0)+\frac{1}{s}\mathcal{L}\left[T_0^*\right]-\frac{1}{s}\mathcal{L}\left\{pT_0^*-p\left[\frac{1}{Pr}\nabla^2 T+\frac{1}{r}\left(\frac{\partial\psi}{\partial r}\frac{\partial T}{\partial\theta}-\frac{\partial\psi}{\partial\theta}\frac{\partial T}{\partial r}\right)\right]\right\}\right] \tag{53}$$

Based on the assumption of HPM, the following was obtained:

$$\psi=\sum_{j=0}^{\infty}p^j\psi_j \text{ and } T=\sum_{j=0}^{\infty}p^jT_j \tag{54}$$

And the nonlinear terms were represented as:

$$\frac{\partial\psi}{\partial\theta}\frac{\partial\nabla^2\psi}{\partial r}=\sum_{j=0}^{\infty}p^jH_j,\frac{\partial\psi}{\partial r}\frac{\partial\nabla^2\psi}{\partial\theta}=\sum_{j=0}^{\infty}p^jH_j^*,\frac{\partial\psi}{\partial\theta}\frac{\partial T}{\partial r}=\sum_{j=0}^{\infty}p^jG_j \text{ and } \frac{\partial\psi}{\partial r}\frac{\partial T}{\partial\theta}=\sum_{j=0}^{\infty}p^jG_j^* \tag{55}$$

Eqs. (54) and (55) were substituted into Eqs. (52) and (53), which obtained:

$$\begin{array}{l}\sum_{j=0}^{\infty}p^j\psi_j=\\ \mathcal{L}^{-1}\left[\begin{array}{l}\frac{1}{s}\psi(0)+\frac{1}{s}\mathcal{L}\left[\psi_0^*\right]-\\ \frac{p}{s}\mathcal{L}\left[\psi_0^*\right]-\frac{p}{S}\mathcal{L}\end{array}\left\{\mathcal{F}^{-1}\left[\frac{1}{i\omega}\mathcal{F}\left(\begin{array}{c}\frac{\partial}{\partial t}\left(\frac{\partial^2}{\partial r^2}\sum_{j=0}^{\infty}p^j\psi_j\right)r+\frac{1}{r}\frac{\partial}{\partial t}\left(\frac{\partial^2}{\partial\theta^2}\sum_{j=0}^{\infty}p^j\psi_j\right)\\ +Gr\left(r\cos(\theta)\frac{\partial}{\partial r}\sum_{j=0}^{\infty}p^jT_j-\sin(\theta)\frac{\partial}{\partial\theta}\sum_{j=0}^{\infty}p^jT_j\right)\\ -\left(\nabla^4\sum_{j=0}^{\infty}p^j\psi_j\right)r-\left(\sum_{j=0}^{\infty}p^jH_j^*-\sum_{j=0}^{\infty}p^jH_j\right)\end{array}\right)\right]\right\}\right]\end{array} \tag{56}$$

$$\sum_{j=0}^{\infty}p^jT_j=\mathcal{L}^{-1}\left[\frac{1}{s}T(0)+\frac{1}{s}\mathcal{L}\left[T_0^*\right]-\frac{p}{s}\mathcal{L}\left[T_0^*\right]+\frac{p}{s}\mathcal{L}\left\{\begin{array}{c}\frac{1}{\mathrm{Pr}}\nabla^2\sum_{j=0}^{\infty}p^jT_j+\\ \frac{1}{r}\left(\sum_{j=0}^{\infty}p^jG_j^*-\sum_{j=0}^{\infty}p^jG_j\right)\end{array}\right\}\right] \tag{57}$$

Coefficients of the same powers of p were compared, which obtained:

$$p^0:\left\{\begin{array}{l}\psi_0=\mathcal{L}^{-1}\left[\frac{1}{s}\psi(0)+\frac{1}{s}\mathcal{L}\left[\psi_0^*\right]\right]\\ T_0=\mathcal{L}^{-1}\left[\frac{1}{s}T(0)+\frac{1}{s}\mathcal{L}\left[T_0^*\right]\right]\end{array}\right. \tag{58}$$

$$p^1:\left\{\begin{array}{l}\psi_1=\mathcal{L}^{-1}\left[-\frac{1}{s}\mathcal{L}\left[\psi_0^*\right]-\frac{1}{s}\mathcal{L}\left[\mathcal{F}^{-1}\left\{\frac{1}{i\omega}\mathcal{F}\left[\begin{array}{c}\frac{\partial}{\partial t}\left(\frac{\partial^2\psi_0}{\partial r^2}\right)r+\frac{1}{r}\frac{\partial}{\partial t}\left(\frac{\partial^2\psi_0}{\partial\theta^2}\right)-(H_0^*-H_0)-\\ \left(\nabla^4\psi_0\right)r+Gr\left(r\cos(\theta)\frac{\partial T_0}{\partial r}-\sin(\theta)\frac{\partial T_0}{\partial\theta}\right)\end{array}\right]\right\}\right]\right]\\ T_1=\mathcal{L}^{-1}\left[-\frac{1}{s}\mathcal{L}\left[T_0^*\right]+\frac{1}{s}\mathcal{L}\left\{\frac{1}{Pr}\nabla^2T_0+\frac{1}{r}\left(G_0^*-G_0\right)\right\}\right]\end{array}\right. \tag{59}$$

$$p^2:\left\{\begin{array}{l}\psi_2=\mathcal{L}^{-1}\left[-\frac{1}{s}\mathcal{L}\left[\mathcal{F}^{-1}\left\{\frac{1}{i\omega}\mathcal{F}\left[\begin{array}{c}\frac{\partial}{\partial t}\left(\frac{\partial^2\psi_1}{\partial r^2}\right)r+\frac{1}{r}\frac{\partial}{\partial t}\left(\frac{\partial^2\psi_1}{\partial\theta^2}\right)-(H_1^*-H_1)-\\ \left(\nabla^4\psi_1\right)r+Gr\left(r\cos(\theta)\frac{\partial T_1}{\partial r}-\sin(\theta)\frac{\partial T_1}{\partial\theta}\right)\end{array}\right]\right\}\right]\right]\\ T_2=\mathcal{L}^{-1}\left[\frac{1}{s}\mathcal{L}\left\{\frac{1}{Pr}\nabla^2T_1+\frac{1}{r}\left(G_1^*-G_1\right)\right\}\right]\end{array}\right. \tag{60}$$

$$p^j:\left\{\begin{array}{l}\psi_j=\mathcal{L}^{-1}\left[-\frac{1}{s}\mathcal{L}\left[\mathcal{F}^{-1}\left\{\frac{1}{i\omega}\mathcal{F}\left[\begin{array}{c}\frac{\partial}{\partial t}\left(\frac{\partial^2\psi_{j-1}}{\partial r^2}\right)r+\frac{1}{r}\frac{\partial}{\partial t}\left(\frac{\partial^2\psi_{j-1}}{\partial\theta^2}\right)-\left(H_{j-1}^*-H_{j-1}\right)-\\ \left(\nabla^4\psi_{j-1}\right)r+Gr\left(r\cos(\theta)\frac{\partial T_{j-1}}{\partial r}-\sin(\theta)\frac{\partial T_{j-1}}{\partial\theta}\right)\end{array}\right]\right\}\right]\right]\\ T_1=\mathcal{L}^{-1}\left[\frac{1}{s}\mathcal{L}\left\{\frac{1}{Pr}\nabla^2T_{j-1}+\frac{1}{r}\left(G_{j-1}^*-G_{j-1}\right)\right\}\right]\end{array}\right. \tag{61}$$

where,

$$\begin{array}{l}H_0=\frac{\partial\psi_0}{\partial\theta}\frac{\partial\nabla^2\psi_0}{\partial r},H_0^*=\frac{\partial\psi_0}{\partial r}\frac{\partial\nabla^2\psi_0}{\partial\theta},H_1=\frac{\partial\psi_0}{\partial\theta}\frac{\partial\nabla^2\psi_1}{\partial r}+\frac{\partial\psi_1}{\partial\theta}\frac{\partial\nabla^2\psi_0}{\partial r} \text{ and } H_1^*=\frac{\partial\psi_0}{\partial r}\frac{\partial\nabla^2\psi_1}{\partial\theta}+\frac{\partial\psi_1}{\partial r}\frac{\partial\nabla^2\psi_0}{\partial\theta}\\ G_0=\frac{\partial\psi_0}{\partial\theta}\frac{\partial T_0}{\partial r},G_0^*=\frac{\partial\psi_0}{\partial r}\frac{\partial T_0}{\partial\theta},G_1=\frac{\partial\psi_0}{\partial\theta}\frac{\partial T_1}{\partial r}+\frac{\partial\psi_1}{\partial\theta}\frac{\partial T_0}{\partial r} \text{ and } G_1^*=\frac{\partial\psi_0}{\partial r}\frac{\partial T_1}{\partial\theta}+\frac{\partial\psi_1}{\partial r}\frac{\partial T_0}{\partial\theta}\end{array} \tag{62}$$

In the porous annulus, the flow field was segmented into three regions: an inner boundary layer located near the inner cylinder, an outer boundary layer located near the outer cylinder, and a core region located between the two layers. Initial solutions found by Pop et al. [8] were used. In addition to the initial and boundary conditions in Eqs. (37) and (38), the solutions of Eq. (58) in the three regions were given as follows:

$$\psi_0^i = 2\sqrt{t}T_i\left(-\eta\,\mathrm{erfc}(\eta) + \frac{1}{\sqrt{\pi}}\left(e^{-\eta^2}-1\right)\right)\sin(\theta), T_0^i = T_i\,\mathrm{erfc}(\eta) \tag{63}$$

$$\psi_0^o = 2\sqrt{t}T_o\left(\xi\,\mathrm{erfc}(\xi) - \frac{1}{\sqrt{\pi}}\left(e^{-\xi^2}-1\right)\right)\sin(\theta), T_0^o = T_o\,\mathrm{erc}(\xi) \tag{64}$$

$$\psi_0^c = \frac{2\sqrt{t}}{\sqrt{\pi}\,(R^2-1)}\left((T_i+RT_o)\,r - (T_o+RT_i)\,r^{-1}\right)\sin(\theta), T_0^c = 0 \tag{65}$$

Then, the solutions of Eq. (59) were given in the following forms:

$$\psi_1^i = \frac{\cos(\theta)}{\sqrt{t}\pi^{3/2}r^2}\left[\begin{array}{c} T_i\left(\begin{array}{r}\pi T_i\left\{\left(\ln(r)r^2+6rt-4t\right)\mathrm{erfc}(\eta) - 8T_it^{\frac{3}{2}}\sqrt{\pi}+2T_it^{\frac{3}{2}}\sqrt{\pi}\right\}\sin(\theta)\\ +\cdots+Grr^2t\cos(\theta)\end{array}\right)e^{-\eta^2}\\ -2\left(\begin{array}{c}\left\{\sqrt{\pi}T_i\left(\sqrt{t}r^2\ln(r)-2t^{\frac{3}{2}}\right)e^{-\eta^2}+\frac{3}{2}\left(r-\frac{1}{3}\right)\sqrt{t}\pi^{\frac{3}{2}}\,\mathrm{erf}\,c^2(\eta)\right\}T_i\\ +\left(\pi^{3/2}\left(\frac{3}{4}t^{\frac{3}{2}}+T_i\sqrt{t}(1-3r)\right)+3T_i\pi\left(r-\frac{2}{3}\right)\right)\mathrm{erfc}(\eta)+\cdots\end{array}\right)\sin(\theta)\end{array}\right] \tag{66}$$

$$T_1^i = \frac{-T_ie^{-\eta^2}}{\sqrt{t}\pi^{3/2}rPr}\left[\begin{array}{c}-4\sqrt{\pi}\,\mathrm{Pr}\,T_it^{\frac{3}{2}}e^{-\eta^2}\cos(\theta) - 4\pi\,\mathrm{Pr}\,T_it(r-1)\,\mathrm{erfc}(\eta)\cos(\theta)\\ +\pi\left(4tPrT_i(r-1)\cos(\theta)+\mathrm{Pr}\left(r^2-r\right)-r^2+r+4t\right)+\\ 4\sqrt{\pi}PrT_it^{\frac{3}{2}}\cos(\theta)\end{array}\right] \tag{67}$$

$$\psi_1^o = \frac{\sin(\theta)}{\sqrt{t}\pi^{3/2}r^2}\left[\begin{array}{l}\pi T_o^2\left\{\begin{array}{l}\left(\frac{r^5}{3}+R^2r^3-Rr^4+\frac{8Rr^2}{3}-4Rt^2-2R\ln(r)tr^2\right)\mathrm{erfc}(\xi)\\ -4\sqrt{\pi}T_o\ln(r)t^{\frac{5}{2}}+2\sqrt{\pi}T_or^3\sqrt{t}\left(-\frac{1}{2}r+R\right)+\cdots+T_oGrr^4t\end{array}\right\}\cos(\theta)e^{-\xi^2}\\ -\left\{\sqrt{\pi}T_o\left(2\ln(r)t^{\frac{3}{2}}r^2-2t^{\frac{5}{2}}+\ln(t)\sqrt{t}\left(Rr^3-\frac{1}{2}r^4\right)\right)e^{-\xi^2}+\cdots\right\}\cos(\theta)+\cdots\\ +\frac{8}{3}t\pi\left(\left(R-\frac{3}{2}r\right)\cos(\theta)+\frac{3}{4}\ln(r)r^2-\frac{3}{4}r^2+\frac{3}{4}t\right)\end{array}\right] \tag{68}$$

$$T_1^o = \frac{T_oe^{-\xi^2}}{\sqrt{t}\pi^{3/2}r\,\mathrm{Pr}}\left[\begin{array}{c}\sqrt{\pi}\,\mathrm{Pr}\,T_ot^{\frac{3}{2}}e^{-\xi^2}\cos(\theta)+\pi\,\mathrm{Pr}\,T_ot(R-r)\,\mathrm{erfc}(\xi)\cos(\theta)\\ -\pi\left(t\,\mathrm{Pr}\,T_o(R-r)\cos(\theta)+\frac{1}{4}\,\mathrm{Pr}(R-r)r-\frac{1}{4}Rr+\frac{1}{4}r^2-t\right)\\ -\sqrt{\pi}\,\mathrm{Pr}\,T_ot^{\frac{3}{2}}\cos(\theta)\end{array}\right] \tag{69}$$

$$\psi_1^c = 0, T_1^c = 0 \tag{70}$$

where, $\eta = \frac{r-1}{2\sqrt{t}}, \xi = \frac{R-r}{2\sqrt{t}}$, T_i and T_o are the inner and outer cylinder temperatures, respectively, and R is the radius ratio.

Then by setting $p = 1$, the analytical approximate solutions ψ and T were given by:

$$\psi = \lim_{N\to\infty}\left(\sum_{j=0}^{N}\psi_j^i + \sum_{j=0}^{N}\psi_j^o + \sum_{j=0}^{N}\psi_j^c\right) \tag{71}$$

$$T = \lim_{N\to\infty}\left(\sum_{j=0}^{N}T_j^i + \sum_{j=0}^{N}T_j^o + \sum_{j=0}^{N}T_j^c\right) \tag{72}$$

6 Results and Discussion

FLT-HPM was applied to the problem of two-dimensional transient natural convection in a horizontal cylindrical concentric annulus bounded by two isothermal surfaces, which obtained analytical results. The impact of the Grashof number and diameter ratio on the analytical results was discussed in this section.

6.1 Streamline and Isotherm Patterns

Streamlines and isotherm contours were used to illustrate the heat transfer within the cylinders. Figure 2 and Figure 3 show the comparison results between this study and some previous studies [4, 9, 11], with $\mathrm{R} = 2, \mathrm{Pr} = 0.71$ and with 10000 and 38800 as the Grashof number values. As shown in these figures, their analytical results are very consistent when the Grashof and Prandtl numbers and the radius ratio have the same values.

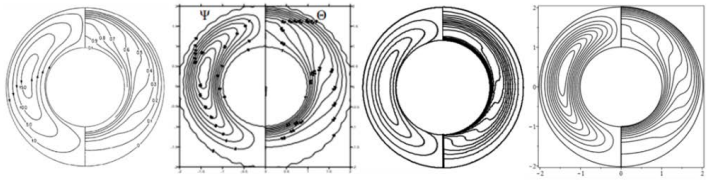

Figure 2. Comparison results between (a) ADI and SOR [4], (b) ADI and SOR [9], (c) YT-HPM [11] and (d) FLT-HPM for stream (left) and isotherm (right) with $\mathrm{Gr} = 10000, \mathrm{Pr} = 0.71$ and $\mathrm{R} = 2$

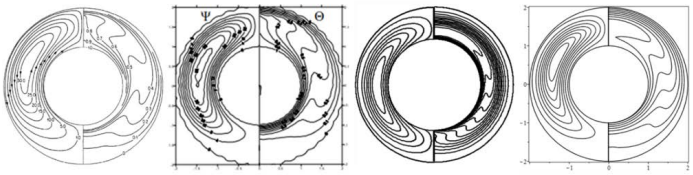

Figure 3. Comparison results between (a) ADI and SOR [4], (b) ADI and SOR [9], (c) YT-HPM [11] and (d) FLT-HPM for stream (left) and isotherm (right), with $\mathrm{Gr} = 38800, \mathrm{Pr} = 0.71$ and $\mathrm{R} = 2$

Table 1. Absolute error comparison of $\psi(r, \theta)$ between FLT-HPM, YT-HPM and HPM with $Gr = 1000, Pr = 0.7$ and $R = 2$

θ	r	***t=0.01***			***t=0.1***		
		FLT-HPM	YT-HPM	HPM	FLT-HPM	YT-HPM	HPM
0	1	0.56×10^{-4}	2.82×10^{-1}	56.983	0.16×10^{-2}	8.921	196.254
	1.5	0.0000	5.44×10^{-4}	1.10×10^{-1}	0.0000	4.775	105.047
	2	2.25×10^{-12}	3.91×10^{-12}	7.91×10^{-10}	0.65×10^{-2}	7.32×10^{-1}	16.109
30	1	0.85×10^{-5}	5.85×10^{-2}	11.811	0.24×10^{-3}	1.463	32.164
	1.5	1.85×10^{-7}	2.09×10^{-4}	4.23×10^{-2}	5.87×10^{-7}	7.54×10^{-1}	16.574
	2	3.46×10^{-8}	1.02×10^{-6}	2.08×10^{-4}	010×10^{-2}	1.03×10^{-1}	2.254
60	1	0.53×10^{-4}	2.64×10^{-1}	53.355	0.15×10^{-2}	8.472	186.363
	1.5	5.73×10^{-8}	6.10×10^{-4}	1.23×10^{-1}	1.81×10^{-7}	4.544	99.954
	2	2.14×10^{-7}	3.69×10^{-7}	6.98×10^{-5}	0.62×10^{-2}	7.01×10^{-1}	15.419
90	1	0.25×10^{-4}	1.39×10^{-1}	28.240	0.93×10^{-3}	4.071	89.597
	1.5	1.68×10^{-7}	2.30×10^{-5}	4.55×10^{-3}	5.31×10^{-7}	2.152	47.371
	2	1.01×10^{-7}	1.01×10^{-6}	1.97×10^{-4}	0.29×10^{-2}	1.18×10^{-1}	7.001
180	1	0.33×10^{-4}	1.65×10^{-1}	31.681	0.98×10^{-3}	5.274	115.973
	1.5	1.50×10^{-7}	6.65×10^{-4}	1.14×10^{-1}	4.76×10^{-7}	2.847	62.603
	2	1.35×10^{-7}	9.24×10^{-7}	1.79×10^{-4}	0.39×10^{-2}	4.48×10^{-1}	9.837

In subgraphs (a) and (b) and (c) of Figure 4, the Grashof number with range ($10^3 \leq Gr \leq 4 \times 10^4$), different radius ratios ($R = 1.2, 1.5$ and 2.0), and Prandtl number of 0.7 were considered.

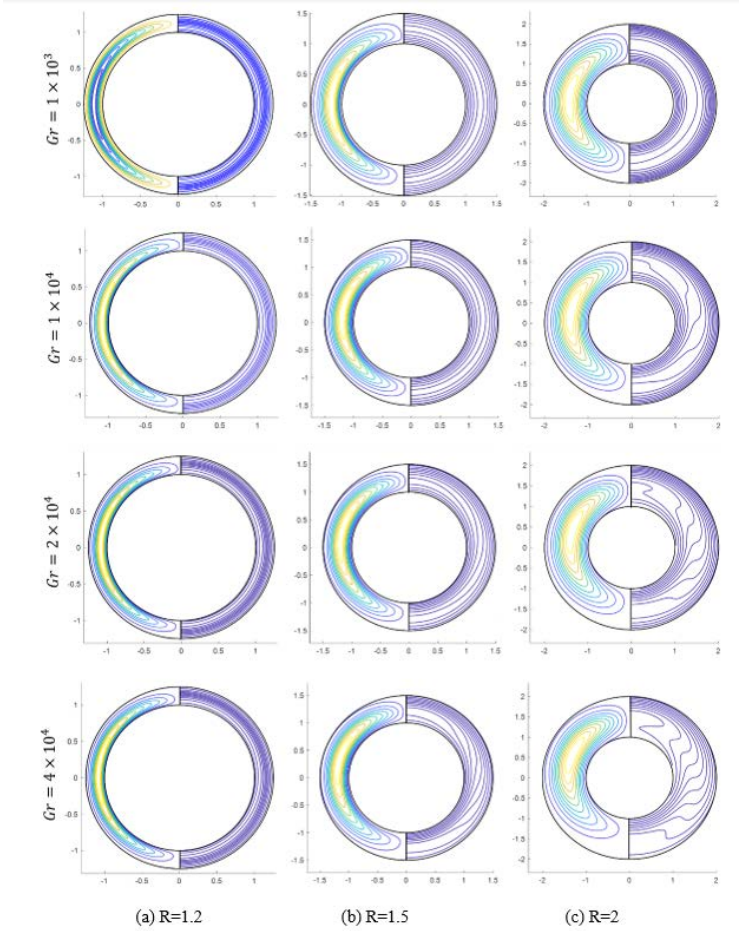

Figure 4. Streamline (left) and isotherms (right) with different values of the Grashof number and $\Pr = 0.7$

According to subgraph (a) of Figure 4, there is no obvious change in the flow pattern and temperature fields with $R = 1.2$ and different values of the Grashof number. In this case, the temperature pattern is similar to circles when the radius ratio is small, indicating the weak effect of thermal currents. When the radius ratio increases to 1.5, the flow pattern starts with an upward displacement in subgraph (b) of Figure 4. In addition, the temperature pattern remains similar to circles when the Grashof number ranges from 10^3 to 10^4, and starts to deform slightly when the Grashof number increases to 4×10^4, indicating the effect of convective currents. Subgraph (c) of Figure 4 illustrates that there is an obvious change in the flow pattern and temperature domains with $R = 2$ and different values of the Grashof number. In this case, the flux gap moves upwards significantly. Moreover, the distortion of the temperature pattern increases when the Grashof number increases to 4×10^4, indicating an increase in the heat convection.

Table 1 and Table 2 show the efficiency and accuracy of the proposed FLT-HPM method in finding approximate analytical solutions to the current problem.

According to the comparison of absolute errors of the approximate solutions in Table 1 and Table 2, the absolute errors of FLT-HPM are less than that of YT-HPM and HPM, with $Gr = 1000$ and $\Pr = 0.7$, which indicates that FLT-HPM has higher accuracy and efficiency than other methods.

6.2 Velocity Distribution

To study the velocity distribution, the velocity component was used in the θ-direction (the tangent velocity), which was calculated by differentiating r in Eq. (71). Figure 5 shows the velocity diagram with $Gr = 1000, \Pr = 0.71, t = 0.01$, different values of the radius ratio $(R = 1.2, 1.5, 2)$, and $\theta = n\,(30^\circ)$, with $1 < n < 5$.

Figure 5 shows the effect of radius ratio on the velocity level in all cases (a, b, and c). It is noted that the absolute maximum values of velocity range from the largest to the smallest when θ is 60°, 120°, 150°, 90°, and 30°, respectively.

Table 2. Absolute error comparison of $T(r,\theta)$ between FLT-HPM, YT-HPM [11] and HPM [11] with $Gr = 1000, \Pr = 0.7$ and $R = 2$

θ	r	***t=0.01***			***t=0.1***		
		FLT-HPM	YT-HPM	HPM	FLT-HPM	YT-HPM	HPM
	1	0.11×10^{-5}	3.25×10^{-3}	17.571	0.28×10^{-4}	3.23×10^{-2}	3.635
0	1.5	1.67×10^{-7}	2.59×10^{-5}	3.38×10^{-3}	0.24×10^{-4}	2.76×10^{-2}	5.73×10^{-1}
	2	1.34×10^{-13}	3.73×10^{-13}	5.59×10^{-11}	0.21×10^{-4}	7.01×10^{-3}	8.58×10^{-2}
	1	021×10^{-5}	1.81×10^{-2}	318.479	0.13×10^{-4}	1.586	380.428
30	1.5	4.96×10^{-8}	2.58×10^{-5}	2.95×10^{-3}	0.28×10^{-4}	2.81×10^{-1}	72.411
	2	1.34×10^{-13}	3.73×10^{-13}	5.59×10^{-11}	2.08×10^{-5}	1.55×10^{-3}	1.183
	1	1.06×10^{-7}	3.48×10^{-3}	115.391	0.27×10^{-4}	4.85×10^{-1}	121.08
60	1.5	1.71×10^{-8}	2.59×10^{-5}	3.99×10^{-3}	0.57×10^{-4}	6.78×10^{-2}	22.358
	2	1.34×10^{-13}	3.73×10^{-13}	5.59×10^{-11}	0.10×10^{-3}	5.51×10^{-3}	2.73×10^{-1}
	1	1.15×10^{-5}	1.22×10^{-2}	282.258	0.28×10^{-5}	1.405	342.265
90	1.5	1.67×10^{-7}	5.59×10^{-5}	4.74×10^{-3}	2.41×10^{-5}	2.91×10^{-1}	65.903
	2	1.34×10^{-13}	3.73×10^{-13}	5.95×10^{-11}	0.22×10^{-4}	1.17×10^{-2}	1.271
	1	1.06×10^{-7}	1.40×10^{-2}	270.701	1.36×10^{-5}	1.289	311.133
180	1.5	4.96×10^{-8}	2.59×10^{-5}	3.44×10^{-3}	0.28×10^{-4}	2.22×10^{-1}	58.827
	2	1.34×10^{-13}	3.73×10^{-13}	5.59×10^{-11}	0.33×10^{-5}	2.69×10^{-3}	9.25×10^{-1}

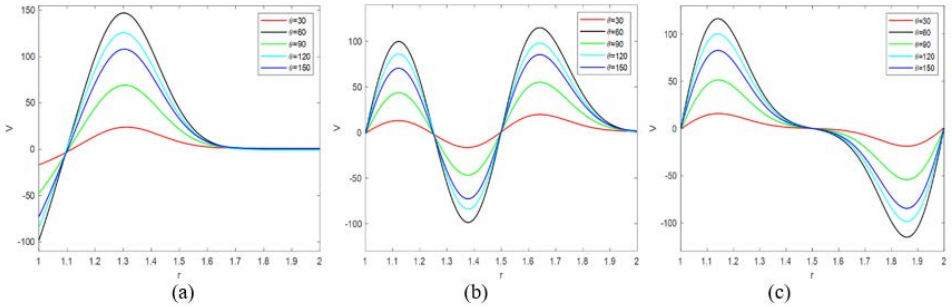

Figure 5. θ-component of velocity versus radial position, with $\theta = \mathrm{n}\,(30^\circ)\,, 1 < \mathrm{n} < 5, \mathrm{Gr} = 1000, \mathrm{Pr} = 0.71, \mathrm{t} = 0.01$, (a) $\mathrm{R} = 1.2$, (b) $\mathrm{R} = 1.5$, and (c) $\mathrm{R} = 2$

6.3 Heat Transfer Rates

Local Nusselt numbers $Nu_i(\theta)$ and $Nu_o(\theta)$ were used to represent the local heat flow rates per unit area in the inner and outer cylinders, respectively. In the same way, the mean Nusselt number $\overline{Nu}$ was used to represent the total heat flow rate from the inner to the outer cylinder. Moreover, the local Nusselt numbers $Nu_i(\theta)$ and $Nu_o(\theta)$, and the mean Nusselt number $\overline{Nu}$ were defined respectively as follows:

$$Nu_i = -\ln(R)\left[r\frac{\partial T}{\partial r}\right]_{r=R_i} \tag{73}$$

$$Nu_o = -\ln(R)\left[r\frac{\partial T}{\partial r}\right]_{r=R_0} \tag{74}$$

$$\overline{Nu_l} = -\frac{\ln(R)}{\pi}\int_0^\pi \left[r\frac{\partial T}{\partial r}\right]_{r=R_i} d\theta \tag{75}$$

$$\overline{Nu_o} = -\frac{\ln(R)}{\pi}\int_0^\pi \left[r\frac{\partial T}{\partial r}\right]_{r=R_o} d\theta \tag{76}$$

Both mean Nusselt numbers $\left(\overline{Nu_l}, \overline{Nu_o}\right)$ vs. the non-dimensional time t were plotted in Figure 6, Figure 7, Figure 8, Figure 9, Figure 10, Figure 11, and Figure 12, with $\Pr = 0.7$ and different values of the Grashof number

and radius ratio. Figure 6, Figure 7, Figure 8 show the mean Nusselt numbers $\left(\overline{Nu_l}, \overline{Nu_o}\right)$, with $R = 1.5, Gr = 4850, Gr = 11500$ and $Gr = 26200$, respectively. According to these figures, when the Grashof number increases, the mean Nusselt numbers $\left(\overline{Nu_l}, \overline{Nu_o}\right)$ also increase with 1.5 as the radius ratio. In addition, Figure 9, Figure 10 and Figure 11 illustrate the mean Nusselt numbers $\left(\overline{Nu_l}, \overline{Nu_o}\right)$, with $R = 2, Gr = 1000, Gr = 38800$ and $Gr = 88000$, respectively. According to these figures, the mean Nusselt number increases when the Grashof number increases with 2 as the radius ratio.

In the above cases in Figure 6, Figure 7, Figure 8, Figure 9, Figure 10, Figure 11, it is noted that when t increases, the mean Nusselt numbers $\left(\overline{Nu_l}, \overline{Nu_o}\right)$ are close to their steady-state values. Furthermore, Figure 12 exhibits the mean Nusselt numbers $\left(\overline{Nu_l}, \overline{Nu_o}\right)$, with $Gr = 732$ and $R = 1.2$, and shows that the mean Nusselt numbers $\left(\overline{Nu_l}, \overline{Nu_o}\right)$ approach unity when t increases, indicating that convection is almost non-existent at the stated values.

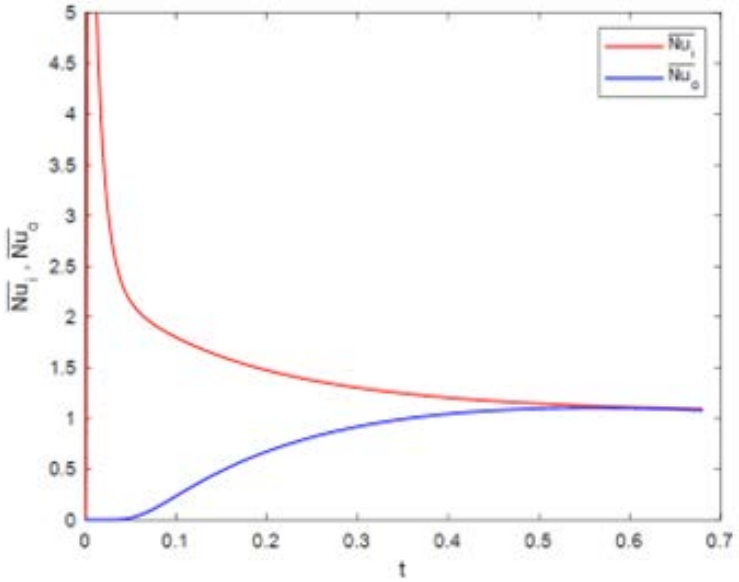

Figure 6. Mean Nusselt number for $\mathrm{Gr} = 4850, \mathrm{Pr} = 0.7$, and $\mathrm{R} = 1.5$

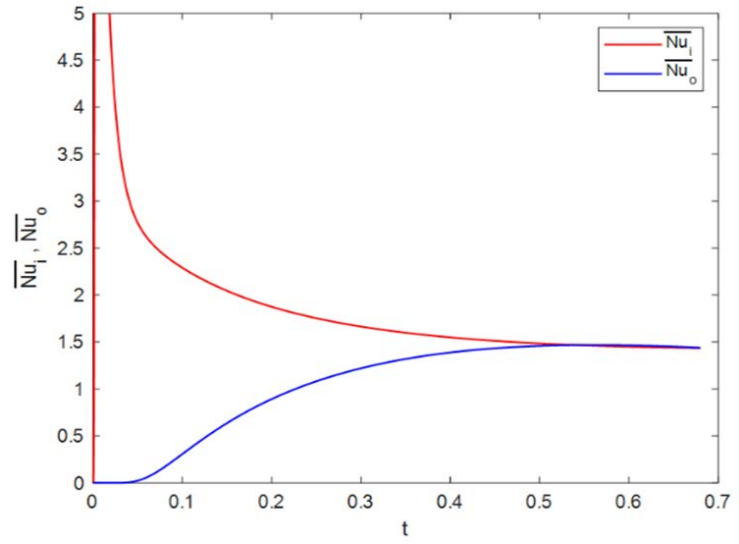

Figure 7. Mean Nusselt number for $\mathrm{Gr} = 11500, \mathrm{Pr} = 0.7$, and $\mathrm{R} = 1.5$

As shown in Table 3, the results of FLT-HPM are very consistent with that of other studies.

7 Convergence analysis of FLT-HPM

Some basic definitions and theorems were presented in this section, which helped the study of convergence analysis. Moreover, this section aimed to find the necessary condition for convergence of approximate analytic solutions using FLT-HPM.

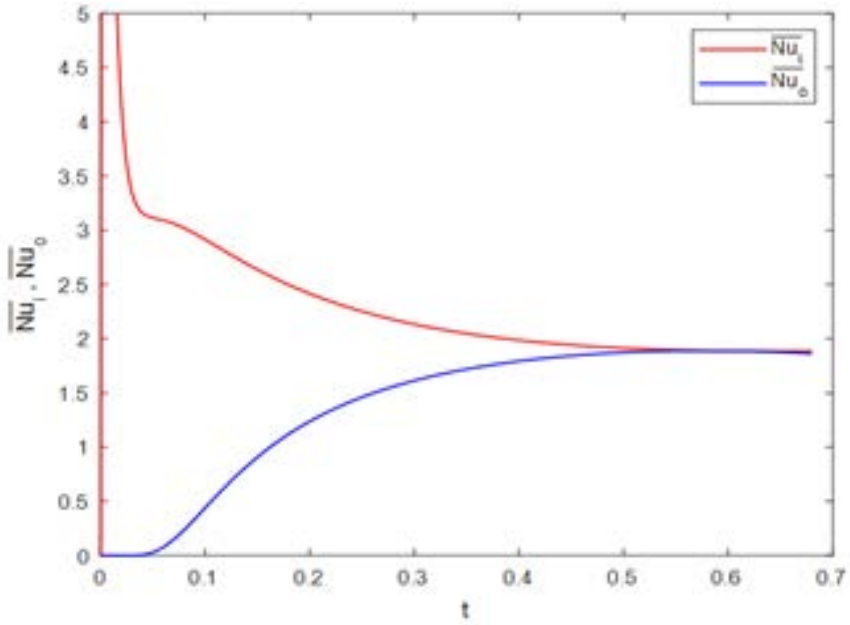

Figure 8. Mean Nusselt number for $\mathrm{Gr} = 26200, \mathrm{Pr} = 0.7$, and $\mathrm{R} = 1.5$

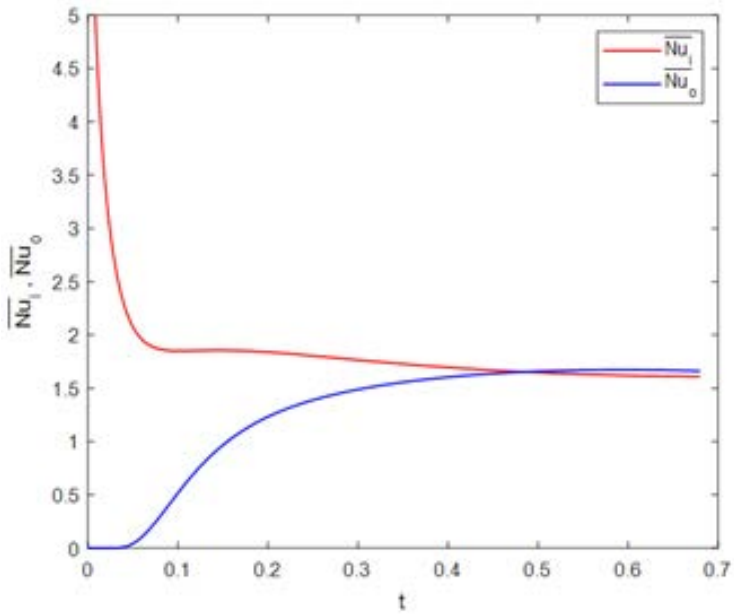

Figure 9. Mean Nusselt number for $\mathrm{Gr} = 10000, \mathrm{Pr} = 0.7$, and $\mathrm{R} = 2$

Table 3. Comparison of the mean Nusselt number of FLT-HPM with ADI and SOR [4] and ADI and SOR [9], at $Pr = 0.7$ and various values of Gr

R	***Gr***	**Mean Nusselt number** $(\overline{\mathbf{Nu}})$		
		FLT-HPM	ADI and SOR [4]	ADI and SOR [9]
2	10000	1.698	1.64	1.658
	38800	2.203	2.4	2.42
	88000	3.06	3.08	2.99

Definition 7.1 Let $\mathcal{T} : H \longrightarrow R$ be a non-linear mapping, where H is the Banach space, and R is the set of real numbers, then the sequence of the solutions was written as:

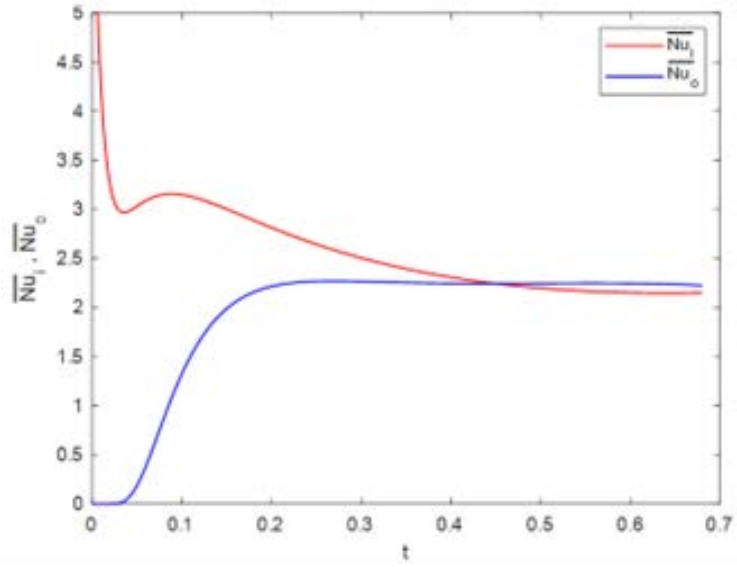

Figure 10. Mean Nusselt number for $\mathrm{Gr} = 38800, \mathrm{Pr} = 0.7$, and $\mathrm{R} = 2$

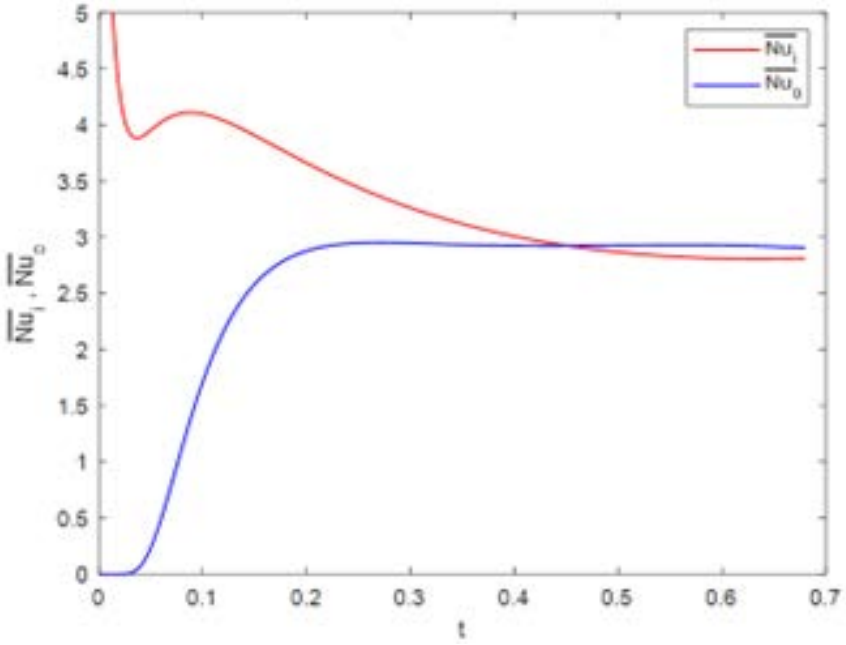

Figure 11. Mean Nusselt number for $\mathrm{Gr} = 88000, \mathrm{Pr} = 0.7$, and $R = 2$

$$E_{n+1} = \mathcal{T}(E_n), E_n = \sum_{j=0}^{n} h_j, j = 0, 1, 2, 3, \ldots \tag{77}$$

where, $\mathcal{T}$ satisfies the Lipschitz condition, and $\gamma \in R$, then there were:

$$\|\mathcal{T}(E_n) - \mathcal{N}(E_{n-1})\| \leq \gamma \|E_n - E_{n-1}\|, \quad 0 < \gamma < 1 \tag{78}$$

Theorem 7.1 The analytical-approximate solution series $\psi(r, \theta) = \sum_{j=0}^{\infty} \psi_j(r, \theta)$, obtained by using FLT-HPM, converge, if the following condition is proven:

$$\|E_{n+1} - E_n\| \to 0 \text{ as } n \to \infty \text{ for } 0 < \gamma < 1 \tag{79}$$

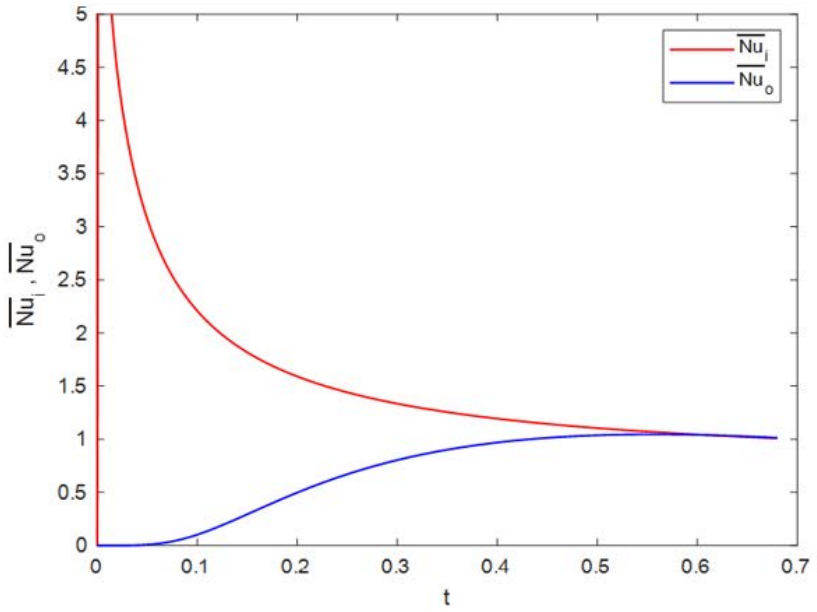

Figure 12. Mean Nusselt number for $\mathrm{Gr} = 732, \mathrm{Pr} = 0.7$, and $\mathrm{R} = 1.2$

Proof of theorem 7.1

$$\begin{aligned}
\|E_{n+1} - E_n\| &= \left\| \sum_{j=0}^{n+1} \psi_j - \sum_{j=0}^{n} \psi_j \right\| = \left\| \psi_0 + \sum_{j=1}^{n+1} \psi_j - \left[\psi_0 + \sum_{j=1}^{n} \psi_j \right] \right\| \\
&= \left\| \psi_0 + \sum_{j=1}^{n+1} L_1^{-1} \left[\mathcal{H}_{j-1} \right] - \left\{ \psi_0 + \sum_{j=1}^{n} L_1^{-1} \left[\mathcal{H}_{j-1} \right] \right\} \right\| \\
&= \left\| \psi_0 + L_1^{-1} \sum_{j=1}^{n+1} \left[\mathcal{H}_{j-1} \right] - \left\{ \psi_0 + L_1^{-1} \sum_{j=1}^{n} \left[\mathcal{H}_{j-1} \right] \right\} \right\|
\end{aligned}$$

Since $E_{n+1} = \mathcal{T}(E_n)$, then

$$\begin{aligned}
\|E_{n+1} - E_n\| &= \left\| L_1^{-1} \mathcal{T} \sum_{j=0}^{n} \left[\mathcal{H}_{j-1} \right] - L_1^{-1} \mathcal{T} \sum_{j=0}^{n-1} \left[\mathcal{H}_{j-1} \right] \right\| = \left\| L_1^{-1} \mathcal{T} \left[\sum_{j=0}^{n} \psi_j \right] - L_1^{-1} \mathcal{T} \left[\sum_{j=0}^{n-1} \psi_j \right] \right\| \\
&\leq \left| L_1^{-1} \right| \left\| \mathcal{T} \left[\sum_{j=0}^{n} \psi_j \right] - \mathcal{T} \left[\sum_{j=0}^{n-1} \psi_j \right] \right\| \leq \gamma \left\| \sum_{j=0}^{n} L_1^{-1} \left[\mathcal{H}_{j-1} \right] - \sum_{j=0}^{n-1} L_1^{-1} \left[\mathcal{H}_{j-1} \right] \right\| \\
&\leq \gamma^2 \left\| \sum_{j=0}^{n-1} L_1^{-1} \left[\mathcal{H}_{j-1} \right] - \sum_{j=0}^{n-2} L_1^{-1} \left[\mathcal{H}_{j-1} \right] \right\| \\
&\vdots \\
&\leq \gamma^n \left\| \sum_{j=0}^{1} L_1^{-1} \left[\mathcal{H}_{j-1} \right] - \sum_{j=0}^{0} L_1^{-1} \left[\mathcal{H}_{j-1} \right] \right\| = \gamma^n \|E_1 - E_0\| \to 0 \text{ as } n \to \infty \text{ for } 0 < \gamma < 1.
\end{aligned}$$

where,

$$L_1^{-1}(\cdot) = \mathcal{L}^{-1} \left[-\frac{1}{s} \mathcal{L} \left(\mathcal{F}^{-1} \left[\frac{1}{i\omega} \mathcal{F}(\cdot) \right] \right) \right], \mathcal{H}_{j-1} = \begin{bmatrix} \frac{\partial}{\partial t} \left(\frac{\partial^2 \psi_{j-1}}{\partial r^2} \right) r + \frac{1}{r} \frac{\partial}{\partial t} \left(\frac{\partial^2 \psi_{j-1}}{\partial \theta^2} \right) - \left(H^*_{j-1} - H_{j-1} \right) - \\ r \nabla^4 \psi_{j-1} + \mathrm{Gr} \left(r \cos(\theta) \frac{\partial T_{j-1}}{\partial r} - \sin(\theta) \frac{\partial T_{j-1}}{\partial \theta} \right) \end{bmatrix}.$$

Theorem 7.2 For the solution series $T(r,\theta) = \sum_{j=0}^{\infty} T_j(r,\theta)$, generated by using FLT-HPM, the necessary condition for their convergence is to fulfill the property represented in Eq. (79):

Proof of theorem 7.2

$$\begin{aligned}
\|E_{n+1} - E_n\| &= \left\| \sum_{j=0}^{n+1} T_j - \sum_{j=0}^{n} T_j \right\| = \left\| T_0 + \sum_{j=1}^{n+1} T_j - \left[T_0 + \sum_{j=1}^{n} T_j \right] \right\| \\
&= \left\| T_0 + \sum_{j=1}^{n+1} L_2^{-1} \left[\ddot{\mathcal{H}}_{j-1} \right] - \left\{ T_0 + \sum_{j=1}^{n} L_2^{-1} \left[\ddot{\mathcal{H}}_{j-1} \right] \right\} \right\| \\
&= \left\| T_0 + L_2^{-1} \sum_{j=1}^{n+1} \left[\ddot{\mathcal{H}}_{j-1} \right] - \left\{ T_0 + L_2^{-1} \sum_{j=1}^{n} \left[\ddot{\mathcal{H}}_{j-1} \right] \right\} \right\|
\end{aligned}$$

Since, $E_{n+1} = \mathcal{T}(E_n)$, then

$$\begin{aligned}
\|E_{n+1} - E_n\| &= \left\| L_2^{-1}\mathcal{T} \sum_{j=0}^{n} \left[\ddot{\mathcal{H}}_{j-1} \right] - L_2^{-1}\mathcal{T} \sum_{j=0}^{n-1} \left[\ddot{\mathcal{H}}_{j-1} \right] \right\| \\
&= \left\| L_2^{-1}\mathcal{T} \left[\sum_{j=0}^{n} T_j \right] - L_2^{-1}\mathcal{T} \left[\sum_{j=0}^{n-1} T_j \right] \right\| \leq \left| L_2^{-1} \right| \left\| \mathcal{T} \left[\sum_{j=0}^{n} T_j \right] - \mathcal{T} \left[\sum_{j=0}^{n-1} T_j \right] \right\| \\
&\leq \gamma \left\| \sum_{j=0}^{n} L_2^{-1} \left[\ddot{\mathcal{H}}_{j-1} \right] - \sum_{j=0}^{n-1} L_2^{-1} \left[\ddot{\mathcal{H}}_{j-1} \right] \right\| \leq \gamma^2 \left\| \sum_{j=0}^{n-1} L_2^{-1} \left[\ddot{\mathcal{H}}_{j-1} \right] - \sum_{j=0}^{n-2} L_2^{-1} \left[\ddot{\mathcal{H}}_{j-1} \right] \right\| \\
&\vdots \\
&\leq \gamma^n \left\| \sum_{j=0}^{1} L_2^{-1} \left[\ddot{\mathcal{H}}_{j-1} \right] - \sum_{j=0}^{0} L_2^{-1} \left[\ddot{\mathcal{H}}_{j-1} \right] \right\| = \gamma^n \|E_1 - E_0\| \to 0 \text{ as } n \to \infty \text{ for } 0 < \gamma < 1.
\end{aligned}$$

where, $L_2^{-1}(\cdot) = \mathcal{L}^{-1}\left[\frac{1}{s}\mathcal{L}(\cdot)\right]$, $\ddot{\mathcal{H}}_{j-1} = \frac{1}{Pr}\nabla^2 T_{j-1} + \frac{1}{r}\left(G^*_{j-1} - G_{j-1}\right)$.

The results of theorems 7.1 and 7.2 were used to calculate the values of the parameter γ^m by constructing the following definition.

Definition 7.2 For $m = 1, 2, 3, \ldots$

$$\gamma^m = \begin{cases} \frac{\|E_{m+1} - E_n\|}{\|E_1 - E_0\|} = \frac{\|h_{m+1}\|}{\|h_1\|}, \|h_1\| \neq 0, m = 1, 2, 3, \ldots \\ 0 \quad , \|h_1\| = 0 \end{cases} \tag{80}$$

Eq. (80) was used to test the convergence of the analytical solutions to the current problem. Moreover, Table 4 shows the convergence of the approximate analytical solutions obtained using FLT-HPM.

Table 4. Powers of γ using FLT-HPM with $\Pr = 0.7, t = 0.1$ and different values of R and Gr

		$\psi(r,\theta)$			$T(r,\theta)$		
Gr	R	γ	γ^2	$\cdots$	γ	γ^2	..
100	1.5	0.303×10^{-2}	0.617×10^{-3}	...	0.172×10^{-3}	0.733×10^{-4}	..
1000		0.289×10^{-3}	0.590×10^{-4}	$\cdots$	0.165×10^{-3}	0.699×10^{-4}	..
100	2	0.178×10^{-2}	0.100×10^{-3}	...	0.146×10^{-3}	0.868×10^{-4}	..
1000		0.176×10^{-3}	0.988×10^{-4}	...	0.146×10^{-3}	0.875×10^{-4}	.

The convergence results of the analytical solutions using FLT-HPM and YT-HPM [11] were compared (Table 5).

According to Table 4 and Table 5, $\gamma^n \to 0$ as $n \to \infty$ when $0 < \gamma < 1$. In addition, the difference in convergence between FLT-HPM and YT-HPM can be observed, which shows that the powers of γ by using FLT-HPM approach zero faster, compared with YT-HPM in Table 5. Therefore, FLT-HPM represents a better convergence than YT-HPM.

Table 5. Comparison of powers of γ between FLT-HPM and YT-HPM [11] with $Gr = 10, \mathrm{Pr} = 0.7, t = 0.1$ and $R = 1.5$

$\boldsymbol{\psi(r,\theta)}$				$\boldsymbol{T(r,\theta)}$			
Method	γ	γ^2	$\cdots$	Method	γ	γ^2	$\cdots$
FLT-HPM	0.534×10^{-1}	0.110×10^{-3}	$\cdots$	FLT-HPM	0.138×10^{-3}	0.587×10^{-4}	$\cdots$
YT-HPM	2.100×10^{-1}	0.608×10^{-2}	$\cdots$	YT-HPM	0.578×10^{-2}	0.500×10^{-3}	$\cdots$

8 Conclusion

A sophisticated analytical procedure was presented in this study, which combined HPM with the Fourier transform and Laplace transform, thus providing approximate analytical solutions to the problem of two-dimensional transient natural convection in a horizontal cylindrical concentric annulus bounded by two isothermal surfaces. The effect of radius ratio and Grashof number on heat transfer, fluid flow, velocity distribution, and Nusselt number was investigated. The effect of Grashof number with the range ($10^3 \leq \mathrm{Gr} \leq 4 \times 10^4$) at three different radius ratios of 1.2, 1.5 and 2 with $Pr = 0.7$ was discussed. This study showed that the change in the flow pattern and the temperature fields was almost very slight at $Gr = 10^3$ with different radius ratios. In addition, the temperature pattern looked like circles. When the Grashof number increased, the flow pattern moved up, while the temperature distribution pattern remained circles when the radius was small. However, the temperature distribution pattern was distorted with the increase in the radius ratio, clearly indicating the increase in convection. The results obtained using FLT-HPM were consistent with the previously published results. In addition, by discussing accuracy and efficiency, it was found that FLT-HPM represented a powerful and effective procedure, which can be used to solve many convection problems with applications in various branches of science and engineering.

Data Availability

The data used to support the findings of this study are available from the corresponding author upon request.

Conflicts of Interest

The authors declare that they have no conflicts of interest.

References

[1] A. M. Jasim, "New analytical study for nanofluid between two non-parallel plane walls (Jeffery-Hamel Flow)," *J. Appl. Comput. Mech.*, vol. 7, no. 1, pp. 213–224, 2021. https://doi.org/10.22055/jacm.2020.34958.2520

[2] T. H. Kuehn and R. J. Goldstein, "An experimental and theoretical study of natural convection in the annulus between horizontal concentric cylinders," *J. Fluid Mech.*, vol. 74, no. 4, pp. 695–719, 1976. https://doi.org/10.1017/S0022112076002012

[3] M. A. Medebber, N. Retiel, A. Aissa, and M. El Ganaoui, "Transient numerical analysis of free convection in cylindrical enclosure," in *International Conference on Materials & Energy, (ICOME'17 and ICOME'18)*. Tiajin, China: EDP Sciences, 2018.

[4] Y. T. Tsui and B. Tremblay, "On transient natural convection heat transfer in the annulus between concentric, horizontal cylinders with isothermal surfaces," *Int. J. Heat Mass Transfer*, vol. 27, no. 1, pp. 103–111, 1984. https://doi.org/10.1016/0017-9310(84)90242-4

[5] L. Zhang, Y. Hu, and M. Li, "Numerical study of natural convection heat transfer in a porous annulus filled with a Cu-nanofluid," *Nanomaterials*, vol. 11, no. 4, p. 990, 2021. https://doi.org/10.3390/nano11040990

[6] L. Crawford and R. Lemlich, "Natural convection in horizontal concentric cylindrical annuli," *Ind. Eng. Chem. Fundam.*, vol. 1, no. 4, pp. 260–264, 1962. https://doi.org/10.1021/i160004a006

[7] L. R. Mack and E. H. Bishop, "Natural convection between horizontal concentric cylinders for low Rayleigh numbers," *Q. J. Mech. Appl. Math.*, vol. 21, no. 2, pp. 223–241, 1968. https://doi.org/10.1093/qjmam/21.2.223

[8] I. Pop, D. B. Ingham, and P. Cheng, "Transient natural convection in a horizontal concentric annulus filled with a porous medium," *J. Heat Transfer*, vol. 114, no. 4, 1992. https://doi.org/10.1115/1.2911911

[9] A. K. Hassan and J. M. Al-lateef, "Numerical simulation of two dimensional transient natural convection heat transfer from isothermal horizontal cylindrical annuli," *J. Eng.*, vol. 13, no. 2, pp. 1429–1444, 2007.

[10] S. Touzani, A. Cheddadi, and M. T. Ouazzani, "Natural convection in a horizontal cylindrical annulus with two isothermal blocks in median position: Numerical study of heat transfer enhancement," *J. Appl. Fluid Mech.*, vol. 13, no. 1, pp. 327–334, 2020. https://doi.org/10.29252/jafm.13.01.30082

[11] A. S. J. Al-Saif and T. A. J. Al-Griffi, "Analytical simulation for transient natural convection in a horizontal cylindrical concentric annulus," *J. Appl. Comput. Mech.*, vol. 7, no. 2, pp. 621–637, 2021. https://doi.org/10.22055/jacm.2020.35278.2617

[12] M. H. Matin, O. Mahian, and S. Wongwises, "Nanofluids flow between two rotating cylinders: Effects of thermophoresis and brownian motion," *J. Thermophys. Heat Transfer*, vol. 27, no. 4, pp. 748–755, 2013. https://doi.org/10.2514/1.T4122

[13] A. S. Rehan and A. Izhar, "Theoretical analysis of unsteady flow between two stretching cylinders with variable physical properties," *Global Sci. J.*, vol. 8, no. 11, pp. 772–784, 2020.

[14] C. Shu, H. Xue, and Y. D. Zhu, "Numerical study of natural convection in an eccentric annulus between a square outer cylinder and a circular inner cylinder using DQ method," *Int. J. Heat Mass Transfer*, vol. 44, no. 17, pp. 3321–3333, 2001. https://doi.org/10.1016/S0017-9310(00)00357-4

[15] C. Shu and Y. D. Zhu, "Efficient computation of natural convection in a concentric annulus between an outer square cylinder and an inner circular cylinder," *Int. J. Numer. Meth. Fluids*, vol. 38, no. 5, pp. 429–445, 2002. https://doi.org/10.1002/fld.226

[16] J. H. He, "A coupling method of a homotopy technique and a perturbation technique for non-linear problems," *Int. J. Non-Linear Mech.*, vol. 35, no. 1, pp. 37–43, 2000. https://doi.org/10.1016/S0020-7462(98)00085-7

[17] J. H. He, "The homotopy perturbation method for nonlinear oscillators with discontinuities," *Appl. Math. Comput.*, vol. 151, no. 1, pp. 287–292, 2004. https://doi.org/10.1016/S0096-3003(03)00341-2

[18] J. H. He, "Homotopy perturbation technique," *Comput. Methods Appl. Mech. Eng.*, vol. 178, no. 3-4, pp. 257–262, 1999. https://doi.org/10.1016/S0045-7825(99)00018-3

[19] J. Singh and Y. S. Shishodia, "A reliable approach for two-dimensional viscous flow between slowly expanding or contracting walls with weak permeability using sumudu transform," *Ain Shams Eng. J.*, vol. 5, no. 1, pp. 237–242, 2014. https://doi.org/10.1016/j.asej.2013.07.001